Steady-State heat transfer through micro-channels in pressurized He II

Pier Paolo Granieri, Bertrand Baudouy, Aurelian Four, F. Lentijo, Alessandro Mapelli et al.

Citation: AIP Conf. Proc. **1434**, 231 (2012); doi: 10.1063/1.4706925
View online: http://dx.doi.org/10.1063/1.4706925
View Table of Contents: http://proceedings.aip.org/dbt/dbt.jsp?KEY=APCPCS&Volume=1434&Issue=1
Published by the American Institute of Physics.

STEADY-STATE HEAT TRANSFER THROUGH MICRO-CHANNELS IN PRESSURIZED HE II

P. P. Granieri[1,2], B. Baudouy[3], A. Four[3], F. Lentijo[3], A. Mapelli[4], P. Petagna[4], and D. Tommasini[1]

[1]CERN, TE Department
Geneva, 1211, Switzerland

[2]EPFL-LPAP, Swiss Federal Institute of Technology
Lausanne, 1015, Switzerland

[3]CEA/Saclay, Irfu/SACM
F-91191, Gif-sur-Yvette, France

[4]CERN, PH Department
Geneva, 1211, Switzerland

ABSTRACT

The operation of the Large Hadron Collider superconducting magnets for current and high luminosity future applications relies on the cooling provided by helium-permeable cable insulations. These insulations take advantage of a He II micro-channels network constituting an extremely efficient path for heat extraction. In order to provide a fundamental understanding of the underlying thermal mechanisms, an experimental setup was built to investigate heat transport through single He II channels typical of the superconducting cable insulation network, where deviation from the macro-scale theory can appear. Micro-fabrication techniques were exploited to etch the channels down to a depth of ~ 16 μm. The heat transport properties were measured in static pressurized He II and analyzed in terms of the laminar and turbulent He II laws, as well as in terms of the critical heat flux between the two regions.

KEYWORDS: Superfluid helium, micro-channels, heat transfer, superconducting cable insulation, MEMS.

Advances in Cryogenic Engineering
AIP Conf. Proc. 1434, 231-238 (2012); doi: 10.1063/1.4706925

INTRODUCTION

The Large Hadron Collider (LHC) particle accelerator at CERN uses superconducting magnets to bend and focus/defocus the high energy particle beam [1]. The magnet cooling, which is ensured by a pressurized He II (He IIp) bath around the coil, must be as effective as possible to cope with the generated or deposited heat loads (e.g. beam loss, or debris of collisions for the magnets close to the interaction regions).

The cable electrical insulation represents the most important thermal barrier for heat extraction from the coil. In order to overcome this limitation, the LHC Nb-Ti superconducting cables were insulated with overlapped polyimide tapes creating μ-channels, therefore featuring He II permeability [2-4]. Furthermore, a new thermally enhanced insulation based on an even more porous wrapping scheme was recently proposed [5]. Its improved He II permeability allows the coil to withstand larger heat depositions, as those associated to the planned LHC luminosity upgrade [6].

The thermal characterization of the LHC standard insulation allowed estimating the thickness of the equivalent channel responsible for He II heat exchange to be around 10 μm [3-4]. Nevertheless, the heat transport through μ-channels in He IIp was not much investigated: few papers report results for cooling channels of several mm [7-8], and to our knowledge the only work investigating channels of hydraulic diameter smaller than 1 mm was [9], down to 56 μm. On the other hand, extensive studies can be found in literature [10] on μ-channels in saturated He II (He IIs).

This work aims at investigating the steady-state heat transfer in He IIp through the μ-channels typical of the cable insulation channels network, *i.e.* with a thickness of dozens of μm, to investigate any possible deviation from the macro-scale theory. The experimental setup relies on μ-fabrication techniques to realize the desired channels. The results of the measurements are analyzed according to the Landau and Gorter-Mellink laws, depending on the dimensions of the channels and heat flux, with a particular emphasis on the critical heat flux separating the two regimes. These results can constitute a basis for the modeling of the heat transfer through superconducting cable insulation.

EXPERIMENTAL SETUP

The experimental apparatus is composed of an upper and lower Pyrex® wafer, bonded together and diced into a rectangular shape, then inserted on one extremity into other Pyrex® pieces. An inner volume is thus created, as shown in FIGURE 1. Several parallel μ-channels, previously etched on the lower wafer, connect the inner volume to the external

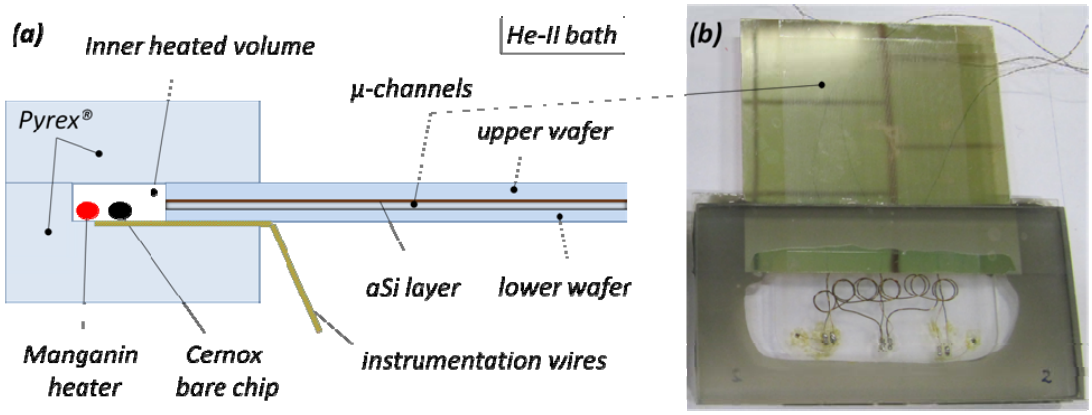

FIGURE 1. Sketch of the experimental setup (a) and picture of sample 2 (b).

bath. The upper wafer is not etched and simply serves as cover. A heater and thermometers are located in the inner volume.

The steady-state temperature increase of the isothermal inner bath is measured and correlated with the dissipated power, thus describing the heat transport through the channel. It is worth noting the importance of having a large number of parallel channels between the same hot and cold sources to increase as much as possible the total cross-sectional area. Since the sample is immersed in the bath, this reduces the ratio of (parasitic) Pyrex® solid conduction with respect to the heat transfer through the channels.

Micro-channels fabrication process-flow

The samples are fabricated in a class 100 clean room. They consist of arrays of 158 to 1000 parallel µ-channels covering an area of 45 mm × 55 mm. The number of channels depends on their width and on the width of the walls separating them. These dimensions vary from one sample to another. Their length is kept constant at 55 mm and the µ-channels are connected via a single inlet distribution manifold and a single outlet. The µ-fabrication process-flow of these devices is illustrated in FIGURES 2. It starts with the etching of the µ-channels in the 525 µm thick lower Pyrex® wafers with a diameter of 100 mm (FIGURE 2(a)). Three different etching techniques are adopted depending on the required depth of the µ-channels. Channels bigger than 20 µm are realized by sandblasting. Channels with dimensions smaller than 20 µm are etched either in an HF solution, or by deep reactive ion etching (DRIE). A 50 nm layer of amorphous silicon (*a*Si) is deposited by sputtering on the surface of the upper wafer (FIGURE 2(b)) that is left unstructured. The two wafers are then anodically bonded to close the µ-channels (FIGURE 2(c)). Finally, the assembly has to be diced into a rectangular shape in order to open the manifolds to the inner volume and to the bath (FIGURE 2(d)).

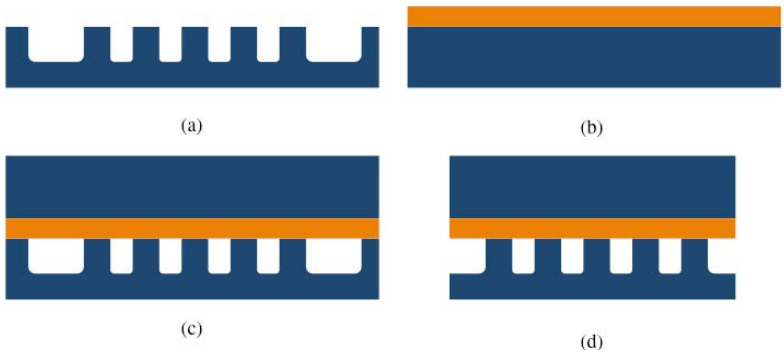

FIGURE 2. Fabrication process-flow. (a) The channels are etched in the lower Pyrex® wafer. (b) A 50 nm *a*Si layer is deposited on the cover (upper) Pyrex® wafer to (c) anodically bond it to the structured wafer. (d) The assembly is diced to open the manifolds to the inner volume and to the bath.

Instrumentation

The inner volume is instrumented with two bare chip Cernox temperature sensors and a Manganin wire heater. The bonded wafers are glued to the other Pyrex® pieces using the 3M® DP190 epoxy resin charged with SiO_2. The instrumentation wires are drawn through small grooves in one of the Pyrex® pieces and sealed into them with the same resin. The He II leak-tightness of the glued and bonded pieces was experimentally verified by testing a sample with no channels (*i.e.* with two bonded cover wafers).

The samples are installed in a Claudet-bath cryostat [11], in horizontal position to eliminate gravitational effect. Measurements are performed in He IIp kept at a constant temperature in the range 1.7-2.0 K and a constant pressure around 1 atm. The temperature difference accuracy is about 0.3 mK, using a lock-in amplifier. The temperature sensors are calibrated in situ in He II. The cryostat bath temperature is regulated and held constant (±1 mK) for the whole test over the range of power dissipation.

SAMPLES

Three samples were realized using the mentioned techniques of sandblasting, HF or DRIE etching. Their geometrical features are summarized in TABLE 1 referring to an equivalent diameter (1) or to the equivalent rectangular cross-section (2 and 3).

TABLE 1. Samples geometrical parameters.

Sample	MEMS technique	Number of channels	Characteristic dimensions (μm)	Total Channels Area (mm^2)	Length (mm)
1	Sandblasting	158	$\Phi_{equivalent}$ = 100.4	1.25	55
2	HF etching	172	17.15 x 75.1	0.22	55
3	DRIE etching	1000	~15.8 x 24	0.38	55

Sample 1 is intended to validate the experimental setup in checking the agreement with the fully developed turbulence theory. Samples 2 and 3 aim at investigating some of the He IIp heat transport features for the first time in channels with a thickness smaller than 20 μm.

Characterization of the channels was carried out using a scanning electron microscope (SEM). As it can be seen in FIGURE 3, the channels realized by sandblasting feature a larger wall roughness (a) (b) than those realized with the HF etching technique (c) (d). They are also less regular: 20% of the sample 1 channels show a deviation from the average cross-section of the order of ±7.5%.

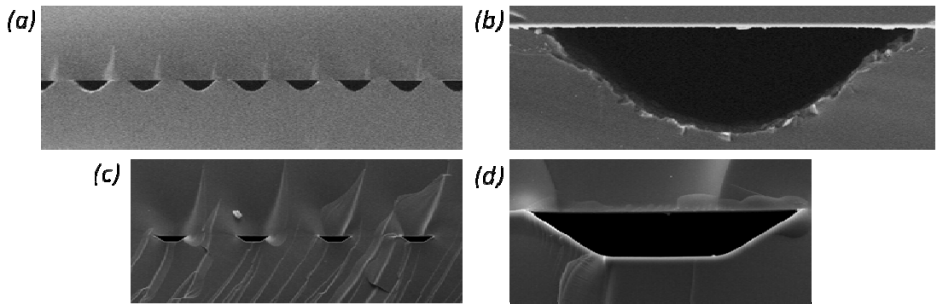

FIGURE 3. Scanning electron microscope (SEM) characterization of sample 1 (a)(b) and sample 2 (c)(d).

Since the SEM characterization is destructive and we plan to perform more measurements with sample 3, the dimensions of its channels have not been measured yet. We have however observed them with an optical microscope and determined a channel width of around 24 μm. The thickness of 15.8 μm reported in TABLE 1 was deduced from heat transfer considerations, as reported in the next section.

RESULTS AND ANALYSIS

Experimental results

FIGURE 4 reports the heat transfer measurements for a bath temperature of 1.9 K, in terms of temperature difference as a function of heat flux. They are compared to theoretical calculation, detailed in the next sub-sections. The laminar and turbulent regimes are clearly identified as well as the transition between them. Sample 1 does not show any transition because of its large dimensions and because our instrumentation is not sensible enough to measure the laminar regime. It can be noticed that Pyrex® solid conduction is not always negligible. We have computed it from [12] for all samples. As an example, thermal conduction through the Pyrex® becomes significant for sample 1 when the data and the calculated curves split. However the analyses reported in the next sub-sections are not affected by it since it has been subtracted from the measured heat flux. Moreover, those analyses were performed in a range of heat flux where the Pyrex® conduction was always below 10% of the measured heat flux to reduce any error that could come from the evaluation of the heat losses.

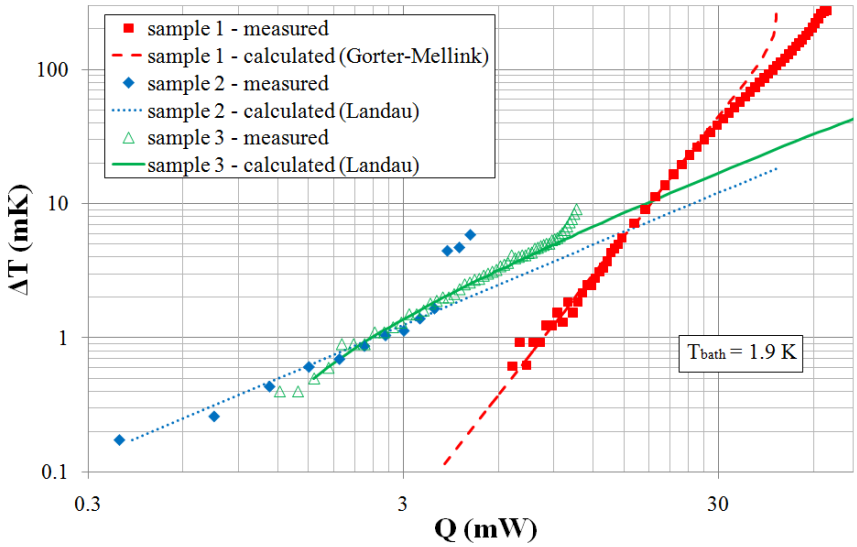

FIGURE 4. Measured thermal gradient as a function of the heat flux at 1.9 K bath temperature for the three samples. The calculations of the Landau and Gorter-Mellink regimes are also reported for comparison.

Turbulent regime

The Gorter-Mellink equation writes $\vec{q}^{\,3} = -\frac{\rho_s^3 s^4 T^3}{A\rho_n}\vec{\nabla}T$, where ρ_s and ρ_n are the density of the superfluid and of the normal components respectively, s is the entropy, T the temperature, A the temperature dependent Gorter-Mellink coefficient. For small ∇T one can calculate A for sample 1 and compare it with values from literature [13], as shown in FIGURE 5. Despite the quite large error bars due to the non uniformity of the channels cross-section, this confirms Kimura's study [9], the only one showing that A does not depend on the geometrical shape and size down to these small dimensions. This result confirms that our set-up is suited to study heat transfer in μ-channels.

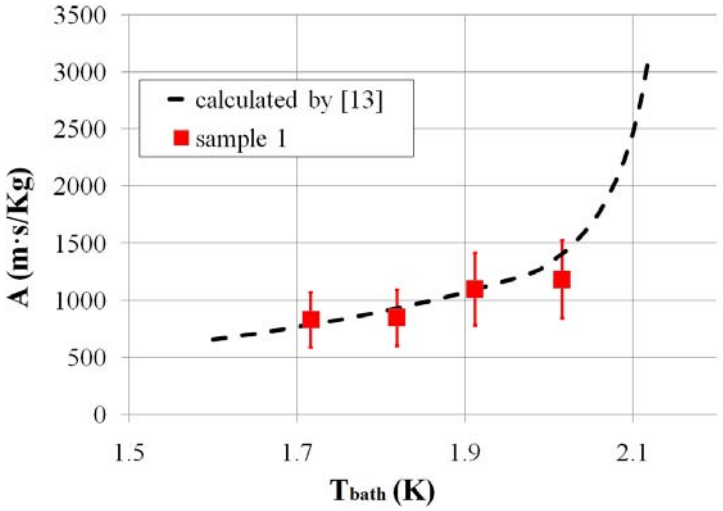

FIGURE 5. Comparison between Gorter-Mellink coefficient derived from data and calculated by [12].

Laminar regime

The Landau equation writes $\vec{q} = -\frac{(\rho s d)^2 T}{\beta \eta} \vec{\nabla} T$, where ρ is the density of the bulk helium, d is the diameter of the tube (if circular), η is the viscosity and β is a coefficient depending of the type of the cross-section of the channel. In the approximation of a rectangular cross-section, the relation between the normal fluid velocity and pressure and temperature gradients [14-15] yields a β of 12 and a d expressed as a combination of the two dimensions of the rectangular cross-section. The laminar part of the measured curves reported in FIGURE 4 for samples 2 and 3 can be reproduced by varying the channels thickness, which determines (together with the width) the parameter d of the above equation. TABLE 2 shows this value is very close to the measured one for sample 2, thus giving confidence on the estimation done for sample 3. Note that for sample 2 at 2.0 K bath temperature the laminar regime does not follow closely the theory and the transition to turbulent regime is no longer sharp, as already observed by other authors [16]. Hence it is not possible to determine d (or Q_{c1}, in next sub-section).

TABLE 2. Channels thickness allowing reproducing the measurements in the Landau regime.

T bath (K)	channels thickness deduced from data vs. Landau equation (μm)	
	sample 2	sample 3
1.7	17.2	15.8
1.8	18.3	16.0
1.9	18.3	15.6
2.0	-	15.8

Critical heat flux identifying the end of the Landau regime (Q_{c1})

The transition between He-II laminar and turbulent regime does not occur all at once but through an intermediate region delimited by the critical heat fluxes Q_{c1} and Q_{c2} [10]. Q_{c1} corresponds to the onset of vorticity in the superfluid component, whereas Q_{c2} to the development of normal component turbulence. Q_{c1} can be identified in our measurements

for samples 2 and 3, and is shown in FIGURE 6 as a function of the bath temperature. As observed in the previous sub-section, at 2.0 K the transition between laminar and turbulent regime is not always as sharp as for lower bath temperatures [16], thus making difficult to estimate Q_{c1}. FIGURE 6 also reports Q_{c1} values predicted by Ladner and Tough [17] in the case of our geometries. They are in rather good agreement with those of sample 2 until the peak at 1.9 K, despite the geometrical and fitting parameters present in [16] that are not known in our case. The bigger difference between data and calculation for sample 3 can be due to these parameters or to the uncertainty on the cross-section, which was considered as the one obtained from the analysis of the Landau regime.

The same behavior as in our tests was also observed by Baudouy [18] in the channels network of superconducting cables electrical insulation, where Q_{c1} featured a peak between 1.9 and 2.1 K before decreasing as approaching T_λ . In terms of the superfluid critical velocity v_{sc}, that is proportional to Q_{c1}, Keller and Hammel showed a v_{sc} independent of temperature in slits of 200 µm and 30 µm thickness, except for temperatures near T_λ where the critical velocity becomes zero [19]. Griffiths [20] showed an increase of v_{sc} up to 1.9 K, whereas Jones described a dependence on the superfluid density, thus decreasing as the temperature approaches T_λ [21].

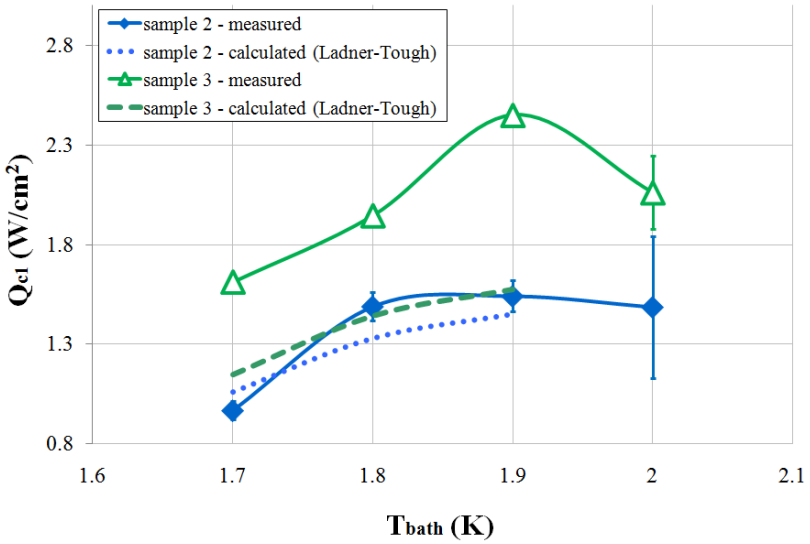

FIGURE 6. Measured critical heat flux Q_{c1} for samples 2 and 3 as a function of the bath temperature. The calculation according to Ladner-Tough's criterion [17] is also reported. Note that the cross section of sample 3 is unknown, therefore we have used the one obtained with the above reported Landau's analysis.

CONCLUSION

We developed a new experimental setup to perform heat transfer measurements through µ-channels in pressurized He-II. We made use of micro electro-mechanical (MEMS) technologies to realize channels similar to those present in the electrical insulation of the LHC Nb-Ti cables, aiming at obtaining a deeper insight of the thermal phenomena occurring in He-II cooled superconducting magnets.

The measurement of the Gorter-Mellink regime in channels with equivalent diameter of ~ 100 µm allowed validating the experimental apparatus, confirming the independence of the heat transfer on the geometrical shape and size down to these dimensions. This result confirms the only study so far carried out in these conditions, then that our set-up is suited to study heat transfer in µ-channels.

In channels of thickness smaller than 20 μm we could identify the Landau regime, as well as the critical heat flux Q_{c1} corresponding to its end. Q_{c1} features an increase until around 1.9 K followed by a decrease towards T_λ , in agreement with some previous works. More measurements are needed to precisely characterize the critical heat flux.

Further investigations are ongoing to reduce the Pyrex® solid conduction in order to allow analyzing the turbulent regime of the smallest channels. Other samples will be tested to provide a systematic analysis as a function of the channel dimension.

ACKNOWLEDGEMENTS

This work is supported by the CERN-CEA-CNRS/IN2P3 collaboration, in the frame of the technical agreement no. 3. We express our gratitude to A. Daël, P. Fessia and V. Parma for their support. We wish to thank some colleagues from CERN for their contribution: the Polymers laboratory (TE-MSC) for assisting in the sample gluing, the Thin films and glass laboratory (PH-DT) for machining the Pyrex® pieces, the Materials and Metrology section (EN-MME) for the sample characterization, the Engineering & Insulation Vacuum section (TE-VSC) for the leak-tightness tests. We are also grateful to the EPFL Center of MicroNanoTechnology (CMI), to B. Lunardi (EPFL-CMI) for helping in the wafers bonding and to D. Solignac (Icoflex Sàrl) for the wafer sandblasting.

REFERENCES

1. Bruning, O., et al., *LHC Design Report vol. 1*, CERN, Geneva, 2004.
2. Meuris, C., Baudouy, B., Leroy, D. and Szeless, B., *Cryogenics* **39**, pp. 921-931 (1999).
3. Baudouy, B., François, M. X., Juster, F.-P. and Meuris, C., *Cryogenics* **40**, pp. 127-136 (2000).
4. Kimura, N., Yamamoto, A., Shintomi, T., Terashima, A., Kovachev, V. and Murakami, M., *IEEE Transaction Applied Superconductivity* **9**, pp. 1097-1100 (1999).
5. Granieri, P. P., Fessia, P., Richter, D. and Tommasini, D., *IEEE Transaction Applied Superconductivity* **20**, pp. 168-171 (2010).
6. Ostojic, R., et al., "Conceptual Design of the LHC Interaction Region Upgrade : Phase-I", LHC Project Report 1163, CERN, Geneva, Switzerland, 2008.
7. Linnet, C., et al., *Journal of Low Temperature Physics* **21**, pp. 447-462 (1975).
8. Khalil, A., et al., *Cryogenics* **23**, pp. 67-71 (1983).
9. Kimura, N., Nakai, H., Murakami, M., Yamamoto, A. and Shintomi, T., "A Study of the Heat Transfer Properties of Pressurized Helium II through Fine Channels", in *Advances in Cryogenic Engineering: Transactions of the Cryogenic Engineering Conference - CEC* 51, edited by J. G. Weisend II, AIP, New York, 2006, pp. 97-104.
10. Arp, V., *Cryogenics* **10**, pp. 96-105 (1970).
11. Baudouy, B. and Polinski, J., *Cryogenics* **49**, pp. 138-143 (2009)
12. Fisher, R. A., Brodale, G. E., Hornung, E. W. and Giaque, W. F., *The Review of Scientific Instruments* **39**, pp. 108-114 (1968).
13. HEPAK, Cryodata, Inc., P.O. Box 173, Louisville, CO 80027.
14. Bejan, A., *Convection Heat Transfer second edition*, John Wiley & Sons, Inc., New York, 1995, p. 105.
15. Van Sciver, S. W., *Helium Cryogenics*, Plenum Press, New York and London, 1986, p. 116.
16. Chase, C. E., *Physical Review* **127**, pp. 361-370 (1962).
17. Ladner, D. R., and Tough, J. T., *Physical Review B* **20**, pp. 2690-2701 (1979).
18. Baudouy, B., "Etude des transferts de chaleur dans les isolations électriques de câbles supraconducteurs d'aimant d'accélérateur refroidi par He superfluide", Ph.D. thesis, Université Paris VI, France, 1996.
19. Keller, W. E. and Hammel, E. F., *Physics* **2**, p. 221 (1966).
20. Griffiths D. J., *Phil. Mag.* **17**, p. 1109 (1968).
21. Jones B. K., *Physical Review* **177**, p. 292 (1969).